European School for Advanced Studies
In Reduction of Seismic Risk

Myths and Fallacies in Earthquake Engineering, Revisited

The Ninth Mallet Milne Lecture, 2003

M.J.N.Priestley
Co-Director

Rose School,
Collegio Alessandro Volta,
Via Ferrata, 27100, Pavia Italy

May 2003

CHAPTER 2: THE ELASTIC STIFFNESS OF CONCRETE MEMBERS

2.1 INTRODUCTION

In section 1.2, problems with the recent tendency towards increased complexity in seismic design were briefly discussed. Amongst these was the incompatibility of refined analysis techniques, such as multimode analysis, with crude approximations to member stiffness, particularly for reinforced concrete and masonry members, where the effects of cracking significantly reduce the stiffness below the initial uncracked value. It was pointed out that the elastic cracked-section stiffness of concrete columns was a function of the axial load ratio, and for columns of a frame structure can vary by as much as +/- 50% or more during seismic response. As a consequence, modal analysis, based on specified, and constant stiffness is unable to provide accurate estimates of seismic forces, even within the elastic range of response. Calculated elastic periods are likely to be in error, and more importantly, the distribution of forces through the structure, which depends on relative stiffness of members, can be grossly in error.

These comments refer to elastic response. It would appear that even greater errors will be induced when the response is inelastic, since some members will remain elastic, while others respond in ductile fashion. Consequently, relative stiffness variations will diverge from the elastic values as inelastic response develops. It would thus seem that what has been termed the *Principle of Consistent Crudeness* has been violated. There is little point in sophisticated analysis if it is based on very coarse and inaccurate data.

The coarseness in stiffness estimates used in seismic design is apparent when different design codes are considered. In many cases, the stiffness is still taken as the gross section (uncracked) stiffness. This would appear to be inappropriate, since cracking of critical elements such as beams will normally have occurred under gravity loading. Even if no previous cracking has occurred prior to the design seismic level of excitation (unlikely, since the probability is that the design level of seismic excitation will be preceded by a number of events of lesser intensity), cracking will occur early, and the stiffness will rapidly reduce. The uncracked stiffness will never be fully regained during, or after the seismic response, and thus is not a useful estimate of effective stiffness.

In other codes, some recognition of the influence of cracking is made, by specifying reduction factors to be applied to the gross-section stiffness. Typically a blanket value of 0.5 is used. In a few codes, notable the New Zealand concrete design code[5], different adjustment factors are specified for different member types. Thus a reduction factor of

0.35 is applied to the gross-section stiffness of beams, while a value between 0.4 and 0.7 is specified for columns. This is clearly an improvement on the use of gross-section values, but is still inadequate to represent stiffness to a degree of precision adequate to justify modal analysis, since the influence of flexural reinforcement ratio is not included.

Regardless of what assumption is made, the member stiffnesses are assumed to be independent of flexural strength. The section stiffness can be assessed from the moment-curvature relationship in accordance with the beam equation:

$$EI = \frac{M_N}{\phi_y} \tag{2.1}$$

where M_N is the nominal moment capacity of the section, and ϕ_y is the yield curvature of the equivalent bilinear representation of the moment-curvature curve. This can be explained with reference to Fig. 2.1, which shows a typical moment-curvature relationship

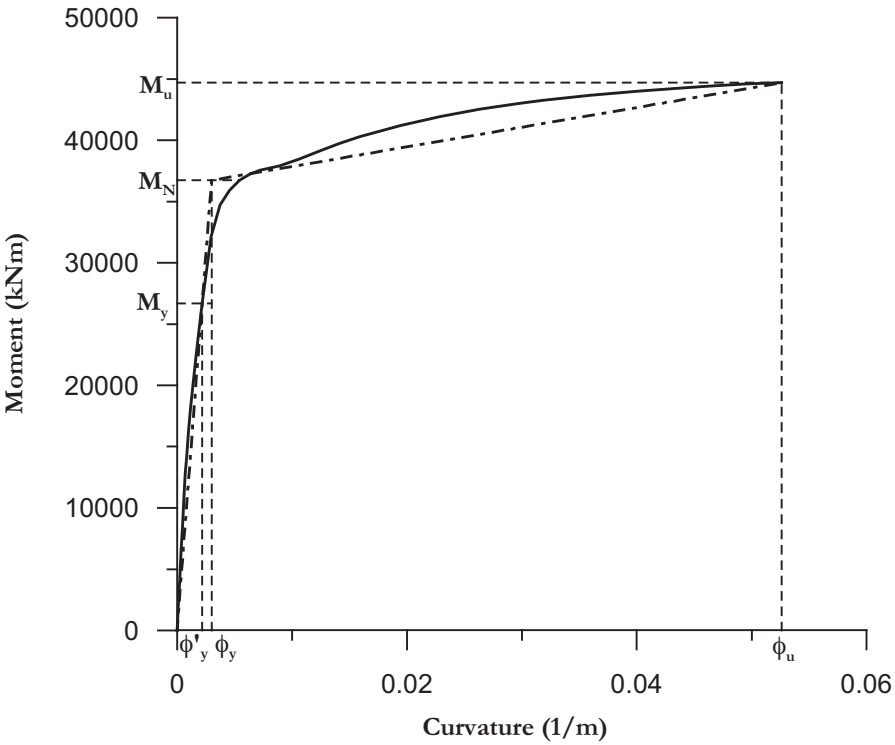

Fig. 2.1 Moment-Curvature Relationship and Bi-Linear Approximation

together with a bilinear approximation. The curve in Fig. 2.1 is the moment-curvature response of a square 1.6m x 1.6m column, with moderate axial load and reinforcement content, and might be appropriate for a bridge column, or the base of a tall building.

It has become accepted by the research community that the most appropriate linearization of moment-curvature relationships is by an initial elastic segment passing through "first yield", and extrapolated to the nominal flexural strength, M_N, and a post-yield segment connected to the ultimate strength and curvature. "First yield" of the section is defined as the moment, M_y and curvature ϕ'_y when the section first attains the reinforcement tensile yield strain of $\varepsilon_y = f_y/E_s$, or the concrete extreme compression fibre attains a strain of 0.002, whichever occurs first. The nominal flexural strength M_N develops when the extreme compression fibre strain reaches 0.004, or the reinforcement tension strain reaches 0.015, whichever occurs first. Thus the yield curvature is given by

$$\phi_y = \phi'_y \left(M_N / M_y \right) \tag{2.2}$$

Member stiffness depends on the distribution of curvature along the entire member length – not just at the critical section where yield will occur. However, experimental evidence indicates that basing the member stiffness on the assumption that curvature varies linearly with moment along the member is adequately accurate. This is partly because slight reductions in curvature, below the linear assumption, for sections with reduced moment are balanced by increased deformation due to shear effects and strain penetration into supporting members. Also, after one or two cycles at or close to yield, the moment-curvature response of all cracked sections up to yield approaches linearity.

Examination of Eq (2.1) reveals that the common design assumption that member stiffness is independent of strength implies that the yield curvature is directly proportional to flexural strength:

$$\phi_y = M_N / EI \tag{2.3}$$

This assumption is illustrated in Fig. 2.2(a). Experimental evidence, and detailed analytical results, indicate that the assumption of stiffness being independent of strength is not valid. In fact, yield curvature is effectively independent of strength, and hence the stiffness is directly proportional to the flexural strength, as is seen from Eq (2.1) with ϕ_y a constant. The correct relationship is thus illustrated in Fig. 2.2(b).

As a consequence of these findings, it is not possible to perform an accurate analysis of either the elastic structural periods, nor of the elastic distribution of required strength through the structure, until the final member strengths have been determined. At the very least, this implies that conventional seismic design, based on elastic member stiffnesses and force-based considerations should be an iterative process, where the member stiffnesses are upgraded during each iteration.

Data justifying the simplistic representation of Fig. 2.2(b) are presented for columns walls, beams and frames in the following sections.

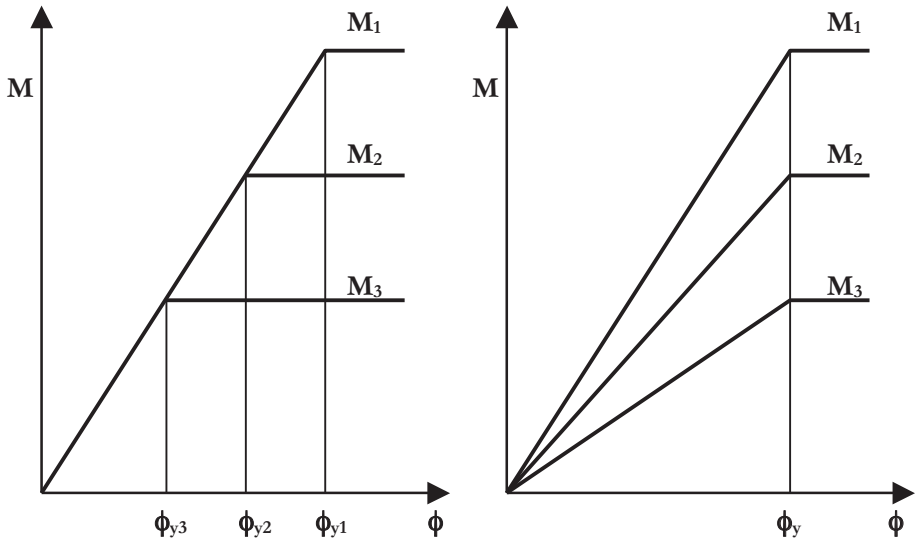

(a) Design Assumption (constant stiffness) **(b) Realistic Conditions (constant yield curvature)**

Fig.2.2 Influence of Flexural Strength on Moment-Curvature Relationship

2.2 ELASTIC STIFFNESS OF CIRCULAR COLUMNS

Circular reinforced concrete columns are the most common lateral force-resisting elements for bridges in seismic regions[4]. In order to investigate the effective stiffness of circular columns, a parameter analysis was carried out varying the axial load ratio and flexural reinforcement ratio for a typical bridge column. The following basic data were assumed:

- Column diameter D = 2m
- Cover to flexural reinforcement = 50 mm
- Concrete compression strength f'_c = 35 MPa
- Flexural Reinforcement diameter = 40 mm
- Transverse reinforcement: spirals = 20mm at 100mm spacing
- Reinforcement yield strength f_y = 450 MPa
- Axial Load Ratio N_u/f'_cA_g = 0 to 0.4 (9 levels)
- Flexural reinforcement Ratio ρ_l/A_g = 0.005 to 0.04 (5 levels)

Analyses were carried out with a program *Cirman4* which represents the section by a minimum of 30 parallel layers. Concrete strains in each layer were calculated from stress-strain relationships that differentiated between cover and core concrete, and considered

the effects of lateral confinement on the concrete compression stress-strain relationship. Reinforcement stress strain characteristics included a yield plateau and strain-hardening effects. Note that concrete confinement and reinforcement strain hardening have comparatively minor effects on the yield curvature or nominal moment capacity, and mainly influence ultimate curvature and ultimate moment (see Fig. 2.1).

A selection of the computed moment-curvature curves is shown in Figs. 2.3 for two levels of flexural reinforcement ratio, and a range of axial load ratios. Only the initial part of the moment-curvature curves has been included, to enable the region up to, and immediately after yield to be clearly differentiated. Also shown in Fig. 2.3 are the calculated bi-linear approximations for each of the curves. Note that the apparent over-estimation by the bi-linear representations of the actual curves is a function of the restricted range of curvature plotted. If the full moment-curvature curve is represented, the agreement is similar to that shown in Fig. 2.1.

It will be seen that the moment capacity is strongly influence by the axial load ratio, and also by the amount of reinforcement. However, the yield curvature of the equivalent bi-linear representation of the moment-curvature curves does not appear to vary much

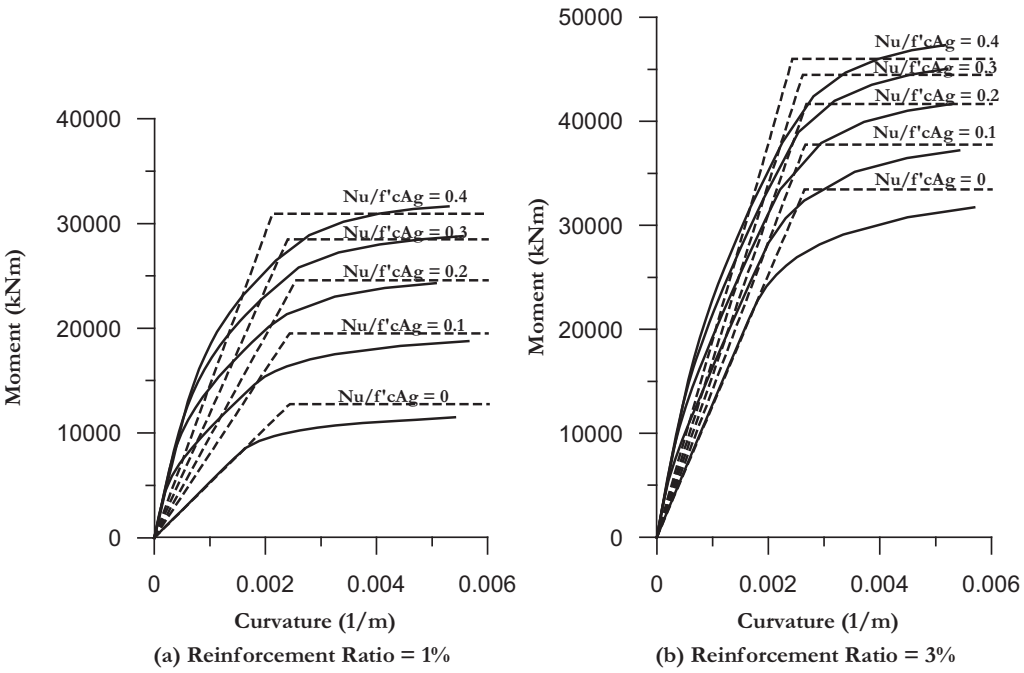

Fig. 2.3: Selected Moment-Curvature Curves for Circular Columns (D=2m, f'_c= 35MPa, f_y = 450MPa)

between the curves.

Data from the full set of analyses for nominal moment capacity, and equivalent bi-linear yield curvature are plotted in dimensionless form in Fig. 2.4. The dimensionless nominal moment capacity is defined as

$$M_{DN} = \frac{M_N}{f'_c D^3} \tag{2.4}$$

and the dimensionless yield curvature as

$$\phi_{Dy} = \phi_y D / \varepsilon_y \tag{2.5}$$

where ε_y is the flexural reinforcement yield strain.

The influence of both axial load ratio and reinforcement ratio on the nominal moment capacity is, as expected, substantial in Fig. 2.4(a), with an eight-fold range between maximum and minimum values. On the other hand, it is seen that the dimensionless yield curvature is comparatively insensitive to variations in axial load or reinforcement ratio. Thus the yield curvature is insensitive to the moment capacity. The average value of dimensionless curvature of ϕ_{Dy} = 2.25 is plotted on Fig 2.4(b), together with lines at 10% above and 10% below the average. It is seen that all data except those for low rein-

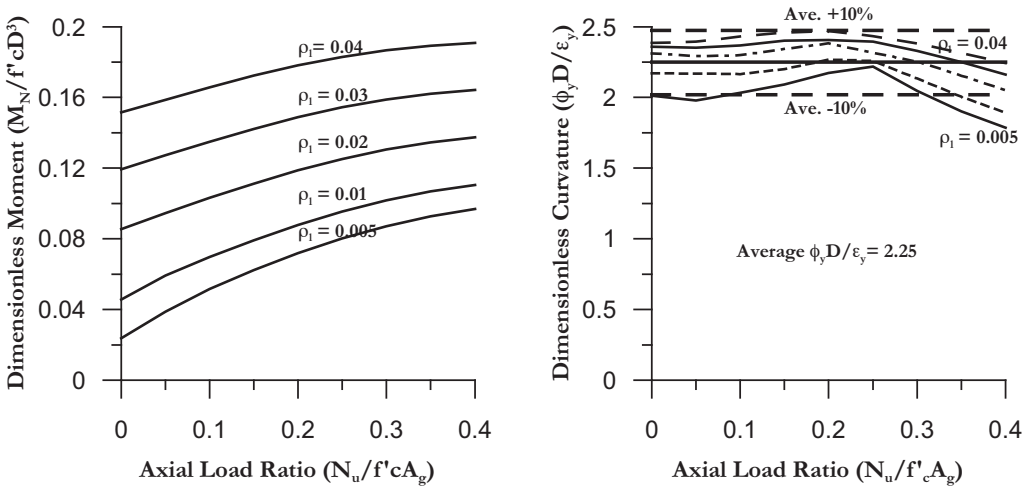

Fig. 2.4: Dimensionless Nominal Moment and Yield Curvature for Circular Bridge Columns

forcement ratio coupled with very high axial load ratio fall within the +/- 10% limits.

It should be noted that though the data were generated from a specific column size and material strengths, the dimensionless results can be expected to apply, with only insignificant errors, to other column sizes and material strengths within the normal range expected for standard design. The results would not, however apply to very high material strengths (say f'_c>50MPa, or f_y>600MPa) due to variations in stress-strain characteristics.

The data in Figs. 2.3 and 2.4 can be used to determine the effective stiffness of the columns as a function of axial load ratio and reinforcement ratio, using Eq. (2.1). The ratio of effective stiffness to initial un-cracked section stiffness is thus given by

$$EI / EI_{gross} = \frac{M_N}{\phi_y EI_{gross}} \tag{2.6}$$

Results are shown in Fig. 2.5 for the ranges of axial load and reinforcement ratio considered. It will be seen that the effective stiffness ratio varies between 0.13 and 0.91.

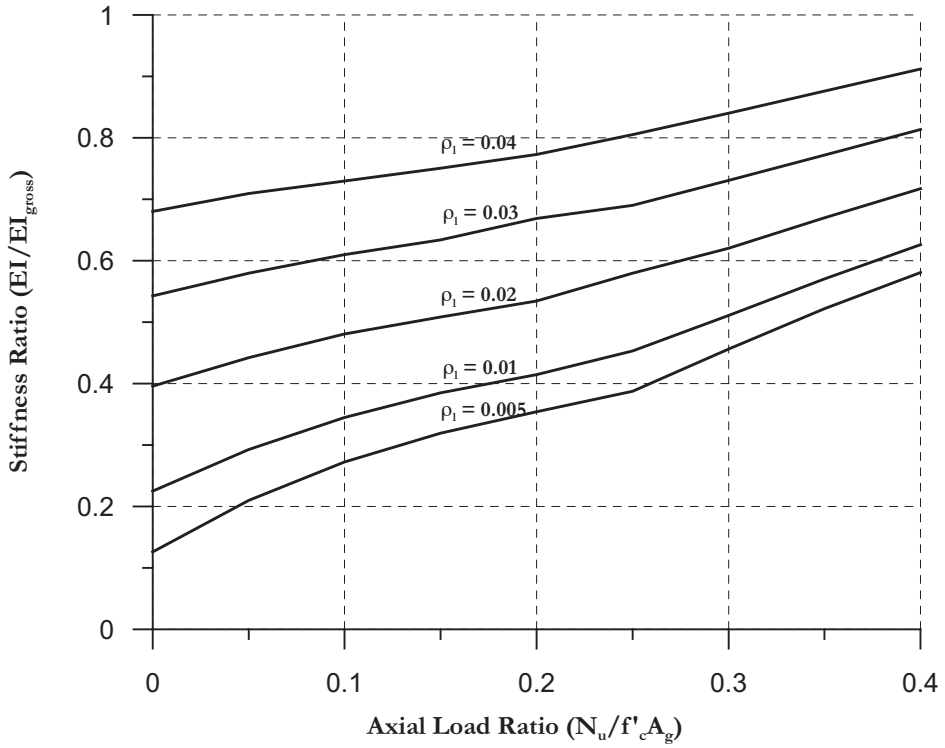

Fig. 2.5: Effective Stiffness of Circular Bridge Columns

It should be noted that for convenience in computing the stiffness ratios of Fig 2.5, the gross stiffness of the un-cracked stiffness has been calculated without including the stiffening effect of the flexural reinforcing steel. That is

$$I_{gross} = \frac{\pi D^4}{64} \tag{2.7}$$

Since the reinforcement increases the un-cracked section moment of inertia by as much as 60% for the maximum steel ratio of 4%, the stiffness ratios related to true un-cracked stiffness would be lower, particularly for the higher reinforcement ratios. The value of the concrete modulus of elasticity used in computing Fig. 2.5 was

$$E = 5000\sqrt{f'_c} \quad \text{(MPa)} \tag{2.8}$$

2.3 ELASTIC STIFFNESS OF RECTANGULAR COLUMNS

A parallel study to that described in the previous section was carried out for rectangular concrete columns. Ductile rectangular columns can occur in bridge design, and at the base of columns of multi-storey frame buildings. For the purposes of this study the special case of a square column with flexural reinforcement evenly distributed around the perimeter was investigated. The following basic data were assumed:

- Column dimensions B = h = 1.6 m
- Cover to flexural reinforcement = 50mm
- Concrete compression strength f'_c = 35 MPa
- Flexural reinforcement diameter = 32 mm
- Transverse reinforcement: hoops = 20mm dia./5 legs
- Reinforcement yield strength f_y = 450 MPa
- Axial load ratio N_u/f'_cA_g = 0 to 0.4 (9 levels)
- Flexural reinforcement ratio ρ_l/A_g = 0.005 to 0.04 (5 levels)

The analyses for rectangular sections were carried out with a program *Recman2* which was based on similar principles to the program *Cirman4* used for the circular analyses of Section 2.2.

A selection of the computed moment-curvature curves for the rectangular sections is presented in Fig. 2.6 for two levels of reinforcement ratio, and a range of axial load ratios. As with the curves for circular columns presented in Fig. 2.3, only the initial part of the moment-curvature curve, up to about 10% of ultimate curvature, but significantly beyond initial yield, has been included. Also shown in Fig. 2.6 are the bilinear representations of the moment-curvature curves based on the principles outlined in Section 2.1 and Fig. 2.1.

The strong influence of axial load ratio and reinforcement ratio on moment capacity apparent for circular sections is also apparent with rectangular sections, as expected.

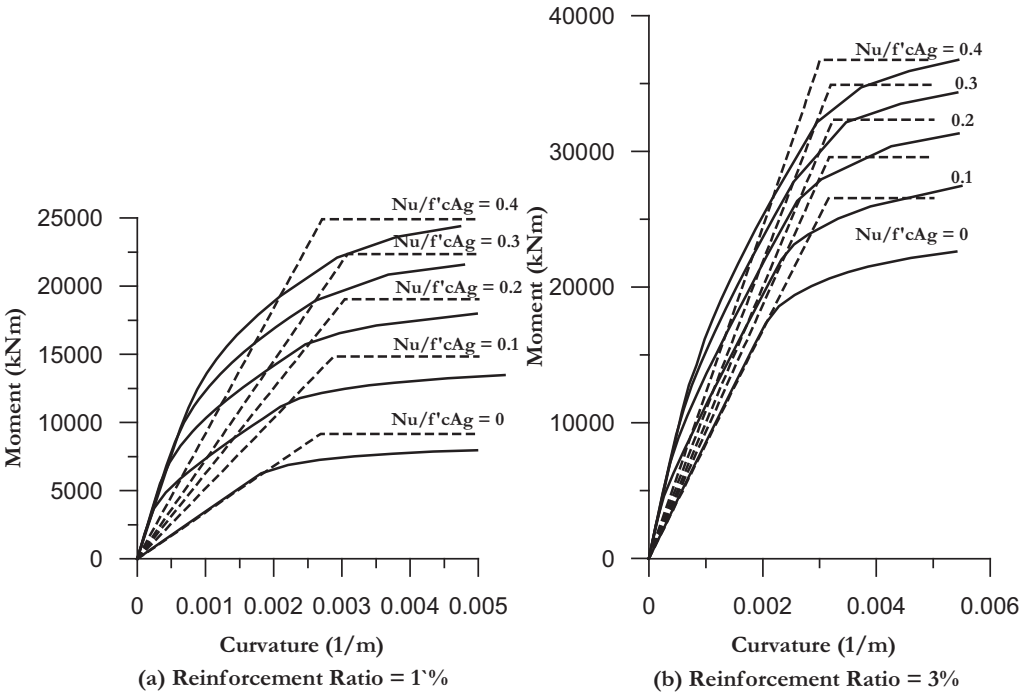

Fig. 2.6 Selected Moment-Curvature Curves for Rectangular Columns (b=1.6m, h_c=1.6m, f'_c= 35MPa, f_y = 450MPa)

Also, as noted for circular sections, the effective yield curvature of the equivalent bi-linear approximation to the moment-curvature relationship does not appear to be significantly dependent on axial load ratio or reinforcement ratio.

Data from the full set of analyses for nominal moment capacity, and equivalent bi-linear yield curvature are plotted in dimensionless form in Fig. 2.7. The dimensionless nominal moment capacity is defined as

$$M_{DN} = \frac{M_N}{f'_c bh^2} \tag{2.9}$$

where b and h are the column width and depth respectively. The dimensionless curvature is

$$\phi_{Dy} = \phi_y h / \varepsilon_y \tag{2.10}$$

Trends for the rectangular columns, apparent in Fig. 2.7, are similar to those displayed in

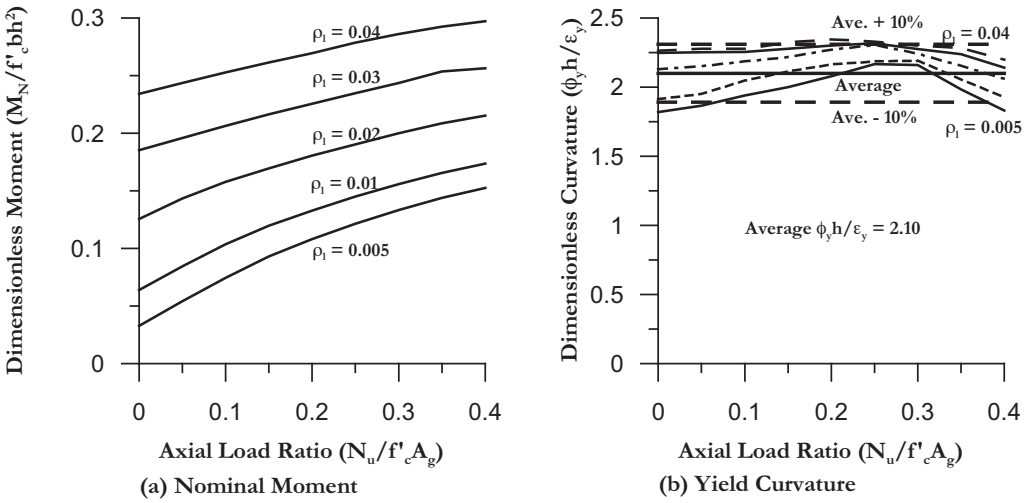

Fig.2.7 Dimensionless Nominal Moment and Yield Curvature for Large Rectangular Columns

Fig.2.4 for circular columns. Nominal moment capacity is strongly dependent on both axial load ratio and reinforcement ratio, with approximately an eight-fold increase in moment capacity from minimum axial load and reinforcement ratio to maximum axial load and reinforcement ratio. Dimensionless yield curvature is only weakly dependent on axial load ratio and reinforcement ratio, thus implying that the yield curvature is insensitive to the nominal moment capacity. The average value of dimensionless curvature of ϕ_{Dy} =2.10 is plotted on Fig.2.7(b), together with lines at 10% above and 10% below the average. It is seen that all data except those for ρ_l =0.005 at both low and high axial load ratio fall within the +/- 10% limits of the average value.

As with the circular columns, the dimensionless results of Fig.2.7 can be expected to apply to other column sizes and material strengths within the normal range of material strengths. Small errors can be expected for small column dimensions, where the ratio of cover to core dimensions will be significantly larger than for the data presented here. As with the circular column data, results should not be applied to rectangular columns with very high strength concrete or reinforcement.

The data of Figs.2.6 and 2.7 have been used to develop curves for the effective stiffness ratio, based on Eq.(2.6). Results are presented in Fig.2.8. For ease of application of the results, the gross-section un-cracked stiffness was computed ignoring the stiffening effect of flexural reinforcement as

$$I_{gross} = \frac{bh^3}{12} \tag{2.11}$$

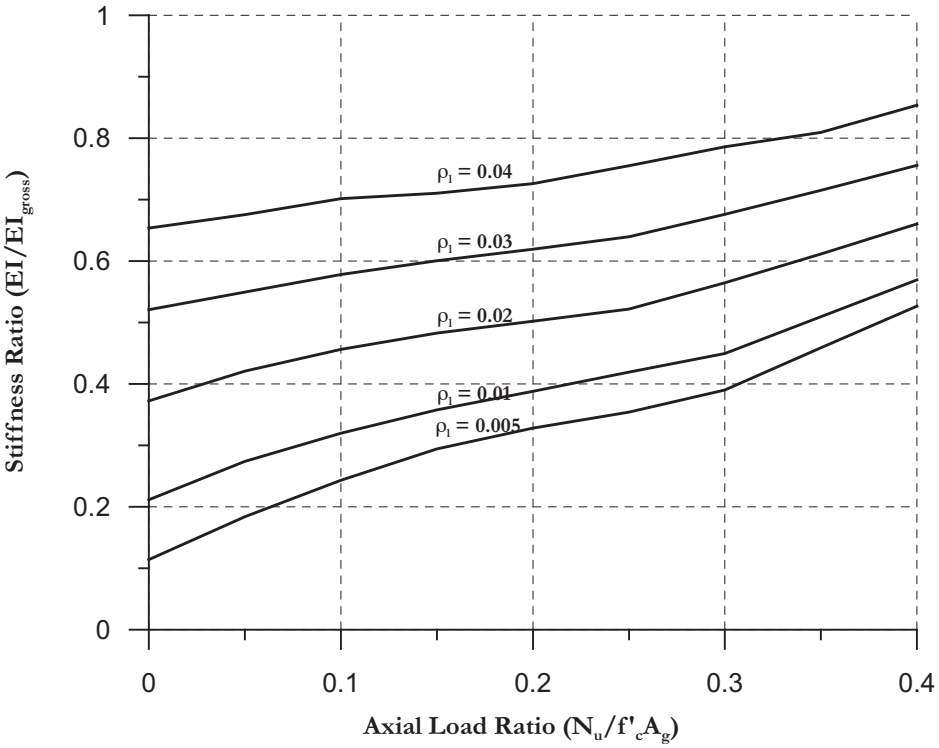

Fig. 2.8 Effective Stiffness of Large Rectangular Columns

Concrete modulus of elasticity was computed using Eq.(2.8).

The range of effective stiffness is from 0.12 to 0.86 times the gross section stiffness, calculated in accordance with Eq.(2.11), indicating the strong dependence of effective stiffness on axial load ratio and reinforcement ratio. Clearly the common assumption of a constant section stiffness independent of flexural strength is entirely inappropriate.

Results from Fig.2.8 can be applied to other column sizes than those used to generate the graph by appropriate substitution of section dimensions into Eq.(2.11).

2.4 ELASTIC STIFFNESS OF RECTANGULAR WALLS

Similar calculations to those reported in the previous two sections can also be carried out for rectangular structural walls, which are common lateral-force resisting elements in seismic design of multi-storey buildings. These have been fully presented elsewhere[6]. Analyses considered two separate cases – one where the flexural reinforcement was distributed uniformly along the wall length, and the second, more common case where most of the flexural reinforcement was concentrated at the wall ends, with a comparatively light reinforcement distributed along the wall length. It is emphasized that

though the latter is the more common case, this is largely because of the misconception that concentrating the flexural reinforcement at the wall ends increases the flexural capacity when compared with the same total amount of reinforcement distributed uniformly along the wall length. In fact, the flexural strength of the two distributions will be almost identical, as simple trial calculations will show. As with the distribution of flexural reinforcement in beams of frame buildings, discussed in Section 1.5, shear performance will be enhanced by uniform distribution of reinforcement, which should thus be preferred over concentration at the wall ends.

Results are presented in Fig.2.9 for the dimensionless yield curvature for walls with different axial load ratios and reinforcement ratios, in similar fashion to the above analyses for columns. However, lower ranges of axial load ratio (with a maximum of N_u/f'_cA_g= 0.12), and reinforcement ratio (with a maximum of ρ_l = 0.02) were adopted since these were considered to be practical upper limits for structural walls. A reinforcement ratio of 0.005 was considered to be uniformly distributed along the wall length, with the remainder concentrated near the wall ends. In Fig.2.9 the yield curvature has been made dimensionless by multiplying by the wall length l_w, and dividing by the yield strain ε_y of the flexural reinforcement, in similar fashion to columns in Eqs.(2.5) and (2.10).

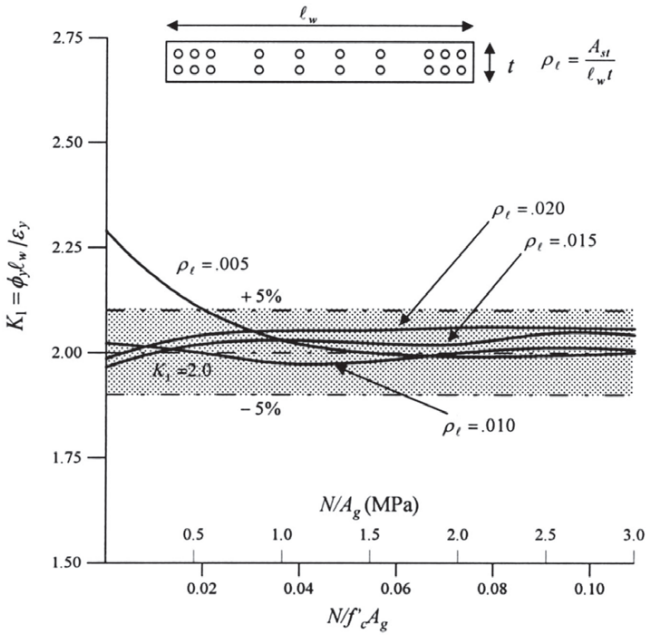

Fig. 2.9: Dimensionless Yield Curvature for Rectangular Walls

An average value of

$$\phi_{Dy} = \phi_y l_w / \varepsilon_y = 2.0 \tag{2.12}$$

is plotted on Fig.2.9, together with lines at average +5% and average –5%. It is seen that except for the case of ρ_l = 0.005 (which in this case means uniformly distributed reinforcement without additional end reinforcement), coupled with low axial load, all data conform to the average +/- 5%.

Analyses where all the flexural reinforcement was distributed uniformly along the wall length resulted in an average dimensionless curvature approximately 10% higher than given by Eq.(2.12), with about twice the scatter of Fig. 2.9[6]. The effective stiffness for rectangular walls can thus be calculated, as a fraction of gross wall stiffness as

$$EI / EI_{gross} = \frac{M_N}{\left(\phi_{Dy}\varepsilon_y / l_w\right)} \cdot \frac{1}{E\left(tl_w^3 / 12\right)} \tag{2.13}$$

where t is the wall width, and M_N is the calculated nominal flexural strength. In Eq. (2.13), ϕ_{Dy} is given by Eq. (2.12) for walls with most of the flexural reinforcement concentrated at the wall ends, or by 1.1 times the value from Eq. (2.12) when all the reinforcement is uniformly distributed along the wall length.

2.5 ELASTIC STIFFNESS OF FLANGED BEAMS

In order to investigate the influence of flexural reinforcement content on the yield curvature and effective stiffness of beams incorporated in ductile building frames, the typical beam section of Fig. 2.10 was considered in an earlier study[7]. Top and bottom

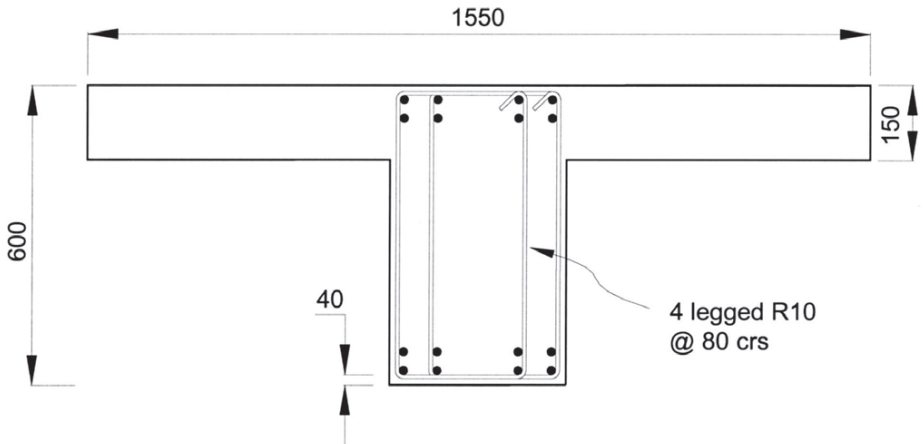

Fig. 2.10: Beam Section Considered for Analysis

reinforcement was placed in either one or two layers. Cover to main reinforcement was 40mm, and a flexural reinforcement bar size of 24 mm was assumed with 24 mm between layers when two layers were used. Tension reinforcement ratios based on an effective depth of 548mm, and the beam width of 350mm, were 0.82%, 1.54% and 2.2%. For top steel, these ratios were taken to include the effective slab contribution. Most analyses were with equal top and bottom reinforcement contents, though one case with 2.2% top reinforcement and 1.1% bottom reinforcement was considered. Reinforcement yield strength was either 300 MPa or 400MPa, and a concrete compression strength of 30 MPa was assumed. The flange width of 1550 mm was considered to be a typical effective width for a monolithic beam/slab construction detail.

Analyses were carried out for both negative bending (top steel in tension) and positive bending (bottom steel in tension). Results of the analyses are included in Tables 2.1 and 2.2. Table 2.1 lists the yield curvatures for both 300 MPa and 400 MPa reinforcement cases under the usual design assumption that strain-hardening is ignored, and for 400 MPa reinforcement including strain-hardening effects. Also included in Table 2.1 are dimensionless curvatures based on Eq.(2.5), substituting the beam depth h_b for the column diameter.

For beam stiffness calculations, the average for negative and positive bending is appropriate as a consequence of moment reversal along the beam length in building frames under seismic loading conditions. Consequently the averaged curvatures, in normal and dimensionless form, are also included for all cases considered, in Table 2.1

Table 2.1: Yield Curvatures for Different Beam Reinforcement Details

Rein-forcement	Bending Case	f_y = 300MPa*		f_y = 400MPa*		f_y = 400MPa**	
		ϕ_y (m^{-1})	$h_b\phi_y/\varepsilon_y$	ϕ_y (m^{-1})	$h_b\phi_y/\varepsilon_y$	ϕ_y (m^{-1})	$h_b\phi_y/\varepsilon_y$
0.82%	Negative	0.00414	1.66	0.00524	1.57	0.00621	1.86
top & bottom	Positive	0.00388	1.55	0.00495	1.49	0.00568	1.70
single layers	Average	0.00401	1.61	0.00510	1.53	0.00595	1.78
1.54%	Negative	0.00444	1.78	0.00571	1.71	0.00674	2.02
top & bottom	Positive	0.00390	1.56	0.00498	1.49	0.00568	1.70
single layers	Average	0.00417	1.67	0.00535	1.60	0.00621	1.86
2.2%	Negative	0.00465	1.86	0.00608	1.83	0.00716	2.15
top & bottom	Positive	0.00388	1.55	0.00513	1.54	0.00587	1.76
single layers	Average	0.00427	1.77	0.00561	1.69	0.00652	1.95
2.2%	Negative	0.00495	1.98	0.00654	1.96	0.00765	2.30
top & bottom	Positive	0.00431	1.72	0.00536	1.61	0.00610	1.83
two layers	Average	0.00463	1.85	0.00595	1.78	0.00688	2.07
2.2% top,2 lrs	Negative	0.00525	2.10	0.00703	2.11	0.00801	2.40
1.1% bottom,	Positive	0.00366	1.46	0.00487	1.46	0.00550	1.65
single layer	Average	0.00446	1.78	0.00595	1.78	0.00676	2.03

* No strain-hardening in analyses ** Strain-hardening included in analyses

Table 2.2: Effective Stiffness Ratios for Different Beam Reinforcement Ratios

Rein-forcement	Bending Case	f_y = 300 MPa		f_y = 400MPa	
		M_N (kNm)	I/I_{gross}	M_N (kNm)	I/I_{gross}
0.82%	Negative	244	0.170	324	0.151
top & bottom	Positive	256	0.190	340	0.173
single layers	Average		0.180		0.162
1.54%	Negative	447	0.291	591	0.299
top & bottom	Positive	469	0.347	622	0.361
single layers	Average		0.319		0.330
2.2%	Negative	632	0.392	838	0.397
top & bottom	Positive	661	0.492	877	0.493
single layers	Average		0.442		0.445
2.2%	Negative	590	0.342	795	0.350
top & bottom	Positive	646	0.433	851	0.458
two layers	Average		0.388		0.404
2.2% top,2 lrs	Negative	603	0.331	778	0.320
1.1% bottom,	Positive	354	0.279	465	0.276
single layer	Average		0.305		0.298

Note: I/I_{gross} based on E = 30 GPa, and $I_{gross} = 0.01155m^4$

As with column and wall analyses reported above, dimensionless yield curvatures vary within a narrow range despite moment capacity variations of more than 250%. If strain-hardening is ignored, and based on the average of positive and negative bending , the dimensionless curvature can be written as

$$\phi_{Dy} = \phi_y h_b / \varepsilon_y = 1.7 \pm 10\% \tag{2.14a}$$

Including the effects of strain-hardening increases the dimensionless yield curvature to

$$\phi_{Dy} = \phi_y h_b / \varepsilon_y = 1.9 \pm 10\% \tag{2.14b}$$

For rectangular-section beams rather than flanged beams, the negative bending results would be applicable for both negative and positive bending, resulting in average values for dimensionless curvature about 10% higher than given by Eq (2.14), and with somewhat increased scatter. It is thus clear that the concept of a constant dimensionless yield curvature for beam sections is an adequate approximation.

Table 2.2 lists nominal flexural strengths for the two cases without strain-hardening, as well as the effective stiffness ratio based on Eq.(2.6), with $I_{gross} = 0.01155m^4$, and E = 30GPa. The stiffness ratio varies between 0.16 and 0.45, with a wider range applicable if negative and positive bending are considered separately. As with columns and walls, the

effective stiffness ratio is highly dependent on the reinforcement ratio, though axial load is not considered relevant for beams in frame design.

2.6 YIELD DRIFTS OF FRAMES

The information provided in the previous sections is sufficient to enable realistic estimates of frame member elastic stiffnesses to be made, provided reinforcement content and axial load ratios are known. It will be noted that since dimensionless yield curvatures can be considered to be constant for a given section type, the effective stiffness can be directly estimated, with considerable accuracy, once the nominal flexural strength is determined, using Eq.(2.1). This would enable refinement of the analysis process for seismic design, when force-based procedures are used.

The comparative invariance of dimensionless yield curvature indicates that yield drift of frames might similarly be essentially independent of reinforcement ratio and strength. Fig.2.11(a) shows a typical beam/column subassemblage extending half a bay width either side of the joint, and half a storey height above and below the joint. This can be considered a characteristic element of a frame building. Since bay width will normally exceed storey height, and column curvatures will typically be less than beam curvatures as a consequence of capacity design procedures[8], beam flexibility is likely to be the major contributor to the deformation.

The deflected shape is shown in Fig.2.11(b). The yield drift θ_y can be expressed as

$$\theta_y = \theta_{by} + \theta_{jy} + 2\Delta_c / l_c + 2\Delta_s / l_c \tag{2.15}$$

where θ_{by} and θ_{jy} are the rotations of the joint center due to beam flexure and joint shear deformation respectively, Δ_c is the flexural deformation of the column top relative to the tangent rotation at the joint center, and Δ_s is the additional deformation of the column top due to shear deformation of beams and columns. To allow for strain penetration of longitudinal reinforcement into the joint region, it is assumed that the yield curvature in the beam develops at the joint centroid, and reduces linearly to zero at the beam midspan, as shown in Fig.2.11(c).

The yield drift due to beam flexure is thus:

$$\theta_{by} = \frac{\phi_y (0.5 l_b)}{3} = \frac{\phi_y l_b}{6} \tag{2.16}$$

Ignoring strain-hardening, and thus substituting from Eq.(2.14(a)):

$$\theta_{by} = 0.283 \varepsilon_y \left[\frac{l_b}{h_b} \right] \tag{2.17}$$

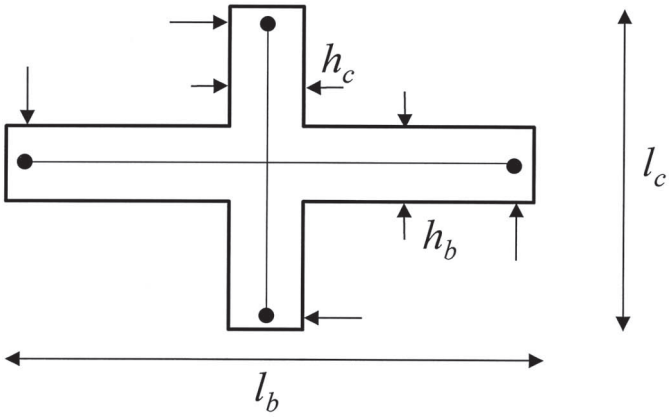

(a) Subassemblage Dimensions

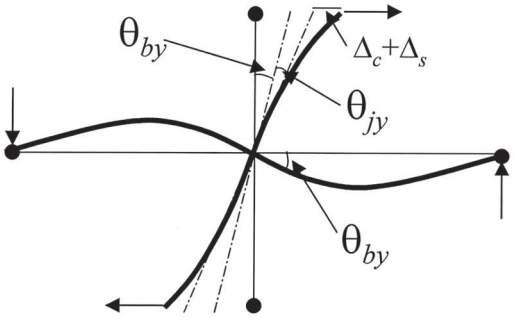

(b) Drift Components

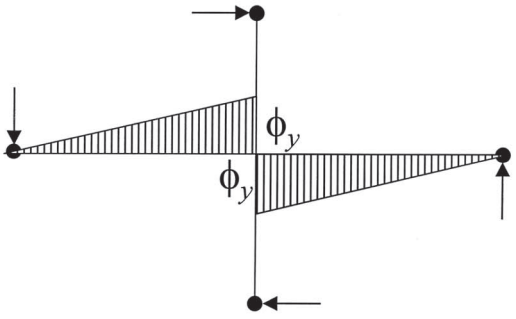

(c) Beam Curvature Distribution

Fig. 2.11: Elastic Deformation Contributions to Drift of a Beam/Column Joint Subassemblage

Typical calculations based on a storey height/bay length ratio of 0.533 (storey height = 3.2m, bay length =6m) and a maximum column curvature of $0.75\phi_y$ indicate column displacement Δ_c will add about 40% to the yield drift in Eq. (2.15). It is further assumed, based on experience, that the joint deformation and member shear deformation add 25% and 10% respectively to the yield drift. As a consequence, the yield drift is predicted to be

$$\theta_y = (1.0 + 0.4 + 0.25 + 0.1) * 0.283\varepsilon_y \left[\frac{l_b}{h_b}\right]$$

$$= 0.5\varepsilon_y \left[\frac{l_b}{h_b}\right] \qquad (2.18)$$

Equation (2.18) is compared in Fig.2.12 with the results from 46 beam/column test assemblages which included a wide range of possibly relevant parameters[7], including

- Column height/beam length aspect ratio (l_c/l_b) : 0.4 – 0.86
- Concrete compression strength (f'_c) : 22.5MPa – 88MPa
- Beam Reinforcement yield strength (f_y) : 276MPa – 611MPa
- Maximum beam reinforcement ratio (A'_s/b_wd) : 0.53% – 3.9%
- Column axial load ratio (N_u/f'_cA_g) : 0 – 0.483
- Beam aspect ratio (l_b/h_b) : 5.4 – 12.6

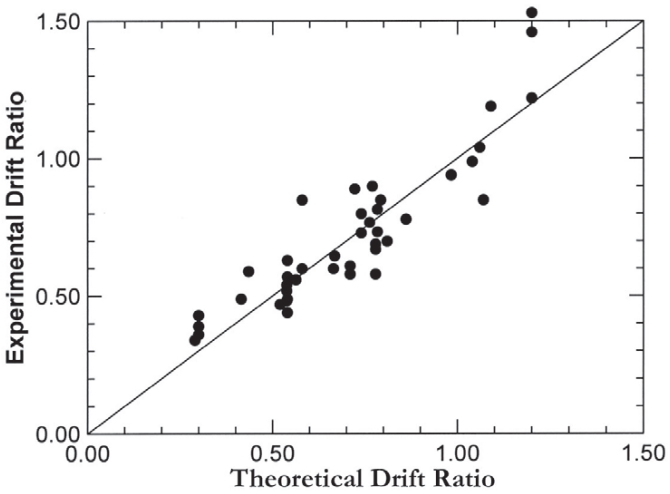

Fig. 2.12 Experimental Drifts of Beam/Column Test Units Compared With Eq.(2.18)

Test units with equal, and with unequal top and bottom reinforcement ratios were considered, as were units with and without slabs and/or transverse beams framing into the joint. Note that Eq.(2.18) only includes two of these parameters (beam reinforcement yield strength (which dictates the yield strain $\varepsilon_y = f_y/E_s$), and beam aspect ratio), on the assumption that the other parameters are not significant variables. Clearly this is an approximation, and some error is expected. It should also be noted that a few test results were discarded because of lack of joint reinforcement and premature joint failure, resulting in excessive yield drifts. Also, a few units with unacceptably high ratios of beam bar diameter to joint depth (d_b/h_c), resulting in slip of beam bars through the joint prior to yield were also discarded. Full details of the test units are available in [7].

As is apparent from Fig.2.12, the agreement between experimental drifts and predictions of Eq.2.18 is reasonable over the full, and rather wide range of yield drifts. The average ratio of experiment to theory is 1.03 with a standard deviation of 0.16. Considering the wide range of parameters considered, the comparatively narrow scatter is rather satisfactory.

In order to examine the sensitivity of the ratio of experimental drift to theoretical drift (θ_E/θ_T) to different potentially significant parameters, it is plotted against reinforcement yield strength, maximum beam reinforcement ratio, beam aspect ratio, and test unit aspect ratio in Figs. 2.13(a), 2.13(b), 2.13(c), and 2.13(d) respectively. In no figure is a strong trend apparent, though there appears to be a trend for θ_E/θ_T to increase with increasing test unit aspect ratio, and to decrease with increasing beam aspect ratio and reinforcement yield strength. Most of these trends are expected: increasing column height relative to beam length will increase the contribution of column deformation to yield drift, and shear deformation will increase for low beam aspect ratio. The extent of the influence is, however, not sufficient to justify increasing the complexity of the very simple Eq.(2.18). Sensitivity to concrete compression strength and column axial load was similarly low[7].

It is of interest to investigate the probable levels of yield drift to be expected in modern design. Examination of Fig.2.12 indicates a range from 0.44% to 1.5%. These are generally much larger than assumed for seismic design. However, many of the test units investigated in Figs. 2.12 and 2.13 have proportions that would be considered unusual for current design practice. If we consider a minimum probable bay length of 6.0m, and a typical beam depth of 600mm, then Eq.(2.18) will predict yield drifts of 1.03% and 1.25% for frames with beam reinforcement of 414MPa (North American practice) and 500MPa (European practice) respectively. Since it is common to specify maximum allowable drifts of between 2.0% and 2.5% under the design level earthquake, the realistic maximum storey drift ductility demand must be in the range of $\mu = 1.6$ to 2.5. Since structural displacement ductility demand will always be less than the drift ductility demand of the critical storey, design ductility levels should be less than these values. As a consequence it will almost never be possible to make full use of the behaviour factors (displacement ductility limits) specified in most seismic design codes, if the drift limits are to be maintained, and realistic estimates of elastic stiffness used.

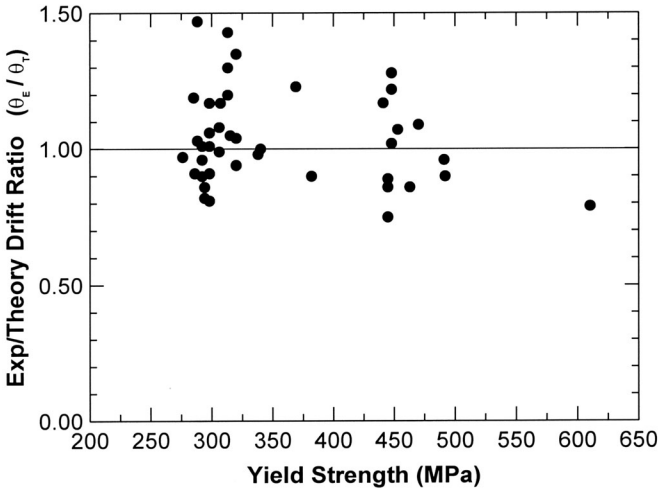

(a) Beam Reinforcement Yield Strength (f_y)

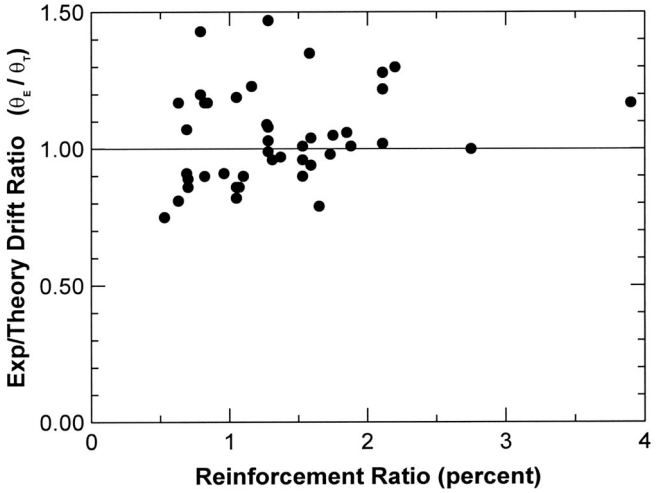

(b) Beam Top Reinforcement Ratio (A'_s/b_wd)

Fig. 2.13 Sensitivity of Experiment/Theory Drift Ratio for Beam/Column Units to Various Parameters, Based on Eq.(2.18)

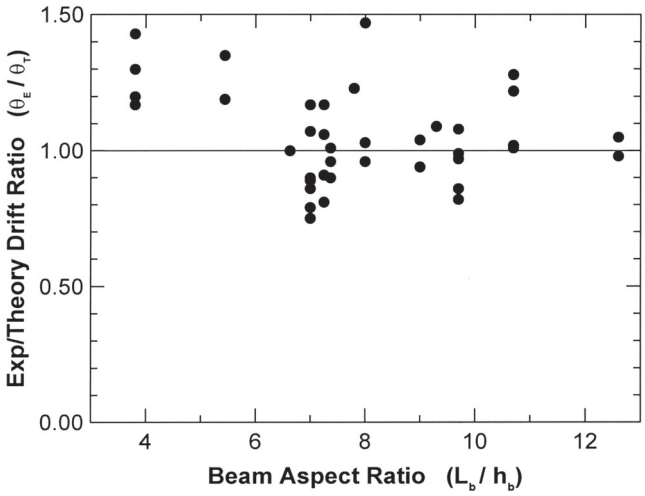

(c) Beam Length/Depth Ratio (L_b/h_b)

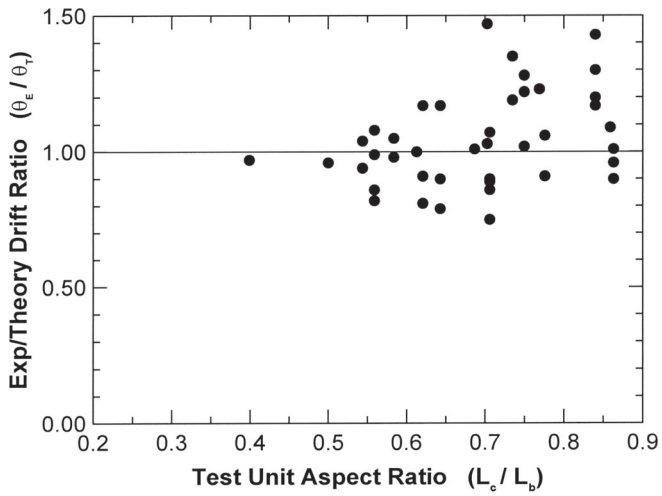

(d) Test Unit Column Height/Beam Length Aspect Ratio

Fig. 2.13 (cont.) Sensitivity of Experimental/Theoretical Drift Ratio for Beam/Column Units to Various Parameters, based on Eq. (2.18)

In order to consider further the implications to current force-based design, we investigate a frame structure with an elastic period estimated as 0.8 seconds, based on initial un-cracked section stiffnesses. As a second consideration, effective stiffnesses of $0.5I_{gross}$ are used, resulting in an elastic period of 1.13 seconds. A realistic assessment of the effective stiffness, based on the approach developed in this chapter, is $0.313I_{gross}$. The displacement ductility for the I_{gross} assumption is $\mu = 6$, and a yield drift of 0.00333 is estimated. Consequently the maximum drift under the design earthquake is 6*0.00333 = 0.02, the code drift limit.

The periods for the other two assumptions of stiffness will be inversely proportion to the square root of the stiffness ratios, and the yield drifts will be inversely proportion to the stiffness ratios. In the medium period range most seismic design codes include acceleration spectra that are based on the assumption of constant spectral velocity. As a result, spectral displacements are directly proportional to period. The relevant period, drift, and ductility values for the three assumptions are thus as summarized in Table 2.3.

Table 2.3. Drift and Ductility Demands of a Frame Designed Based on Un-cracked Section Stiffnesses

Stiffness Assumption	Period (seconds)	Maximum Drift	Yield Drift	Displacement Ductility
$\mathbf{I_{gross}}$	0.80	0.0200	0.00333	6.00
$\mathbf{0.5I_{gross}}$	1.13	0.0283	0.00667	4.26
$\mathbf{0.313I_{gross}}$	1.43	0.0358	0.0107	3.36

It will be noted that the yield drift for the most realistic stiffness assessment at 0.0107 is within the expected range in accordance with Eq.(2.18). Although the frame has been designed for an artificially low period, and hence an apparently high base shear force, the consequence is not a conservative design, but one that results in unacceptably high drifts. Using the "best estimate" of stiffness based on Eq.(2.18), the maximum drift will be nearly 80% above the code drift limit.

2.7 CONCLUSIONS

Analytical and experimental results indicate that current force-based design using an assumed constant fraction of gross-section stiffness for reinforced concrete members, regardless of flexural reinforcement content or axial load level results in excessive errors in period, and in force distribution between members. It was found that stiffness and strength are effectively proportional, for a given structural member type and size, or structure type. The independent parameter, for stiffness calculations, is thus the yield curvature, or yield displacement. The following yield curvatures are applicable for the "corner" of the equivalent bi-linear approximation of force/deformation response:

- Circular column: $\phi_y = 2.25\varepsilon_y / D$ (2.19a)
- Rectangular column: $\phi_y = 2.10\varepsilon_y / h_c$ (2.19b)
- Rectangular cantilever walls: $\phi_y = 2.00\varepsilon_y / l_w$ (2.19c)
- T-Section Beams: $\phi_y = 1.70\varepsilon_y / h_b$ (2.19d)

For reinforced concrete frames, the yield drift can be expressed, with adequate accuracy as

$$\theta_y = 0.5\varepsilon_y \frac{l_b}{h_b} \tag{2.20}$$

It is noted that the analyses reported in this chapter identify a fundamental problem with current force-based design:

Design: Strength is allocated in proportion to stiffness
Analysis: Stiffness is proportional to strength

?